

Excited-State Adiabatic Quantum Computation Started with Vacuum States

Hayato Goto and Taro Kanao

Frontier Research Laboratory, Corporate Research & Development Center,
Toshiba Corporation, 1, Komukai Toshiba-cho, Saiwai-ku, Kawasaki-shi, 212-8582, Japan

(Dated: November 3, 2021)

Adiabatic quantum computation (AQC), which is particularly useful for combinatorial optimization, becomes more powerful by using excited states, instead of ground states. However, the excited-state AQC is prone to errors due to dissipation. Here we propose the excited-state AQC started with the most stable state, i.e., the vacuum state. This counterintuitive approach becomes possible by using a driven quantum system, or more precisely, a network of Kerr-nonlinear parametric oscillators (KPOs). By numerical simulations, we show that some hard instances, where standard ground-state AQC with KPOs fails to find their optimal solutions, can be solved by the present approach, where nonadiabatic transitions are rather utilized. We also show that the use of the vacuum state as an initial state leads to robustness against errors due to dissipation, as expected, compared to the use of a really excited (nonvacuum) state as an initial state. Thus, the present work offers new possibilities for quantum computation and driven quantum systems.

I. INTRODUCTION

Adiabatic quantum computation (AQC) [1–3] or quantum annealing [4–6] is an alternative approach to quantum computation. The AQC is particularly useful for combinatorial optimization problems, where we have to minimize (or maximize) functions of discrete variables called objective (or cost) functions [7]. The Ising problem (search for ground states of Ising spin models) [8, 9] is a typical example of such problems. Ising machines, which are designed for solving the Ising problem, based on AQC are expected to be useful for practical applications, because there are various situations requiring to solve combinatorial optimization problems which can be mapped to the Ising problem [10–12].

The idea of AQC is simple. We start with the ground state of an initial Hamiltonian, where we know the ground state because the initial Hamiltonian is simple enough. Changing the Hamiltonian slowly to the one corresponding to the objective function for a given problem, we finally obtain the ground state of the final Hamiltonian assuming that the quantum adiabatic theorem [13] holds. The final ground state gives us the solution of the problem. There is, however, a problem. If the energy gap between the ground and first excited states almost closes during the AQC, the adiabatic theorem does not hold, and consequently we cannot find the ground state. Thus, the energy-gap closing is a fatal problem for AQC.

One of the approaches to this crucial problem is to use excited states in AQC. For instance, we can achieve an exponential quantum speedup by using an excited state via nonadiabatic transitions at energy-gap closing points during AQC [14]. Moreover, it is known that “stoquastic” AQC [3, 15], to which we can apply a classical simulation method [5], becomes as powerful as universal quantum computation by using excited states [3, 16]. That is, the use of excited states makes AQC more powerful. The positive use of excited states in AQC, where the initial state is intentionally set to an excited state, not the ground state, has been proposed [17]. However, this ap-

proach is accompanied by the problem that the initial state is prone to errors due to dissipation.

In this paper, we propose a new approach to the excited-state AQC, where the initial state is the most stable state, i.e., the vacuum state. This counterintuitive approach is possible by using a driven quantum system, or more precisely, a network of Kerr-nonlinear parametric oscillators (KPOs). The concept of the KPO and quantum computations with KPOs, both the AQC and gate-based universal quantum computation, were proposed in Refs. 18 and 19, which were discovered inspired by a more classical approach using optical parametric oscillators [20–23]. The proposals have been followed by interesting related works, such as superconducting-circuit implementations of KPOs, generation of Schrödinger cat states using KPOs, and theoretical studies on KPOs as new driven quantum systems [24–42]. The characteristic feature of the AQC with KPOs is the use of the *effective* Hamiltonian for the driven system, which enables the vacuum state to be an excited state of the Hamiltonian used for AQC. This intriguing property of driven systems was exploited for preparing quasienergy excited states of a KPO via quantum adiabatic evolution started with the vacuum state [25]. This is the essential point for our approach.

This paper is organized as follows. In Sec. II, we briefly describe standard ground-state AQC with KPOs, and show simulation results in order to clarify the energy-gap closing problem. In Sec. III, we explain the proposed approach, that is, the excited-state AQC started with vacuum states, and demonstrate the usefulness of this approach. In Sec. IV, we examine the effects of dissipation using numerical simulations, where AQC started with a really excited (nonvacuum) state is also simulated for comparison. In Sec. V, we briefly summarize the present work.

II. GROUND-STATE AQC WITH KPOS

The N -spin Ising problem with coupling coefficients $\{J_{i,j}\}$ and local fields $\{h_i\}$ is to find a spin configuration minimizing the (dimensionless) Ising energy defined as

$$E_{\text{Ising}} = -\frac{1}{2} \sum_{i=1}^N \sum_{j=1}^N J_{i,j} s_i s_j - \sum_{i=1}^N h_i s_i, \quad (1)$$

where s_i is the i th spin taking 1 or -1 , and the coupling coefficients satisfy $J_{i,j} = J_{j,i}$ and $J_{i,i} = 0$.

The standard ground-state AQC with KPOs is as follows. To solve the Ising problem, we use a KPO network defined by the following Hamiltonian [18, 20, 31, 43]:

$$H(t) = \hbar \sum_{i=1}^N \left[\frac{K}{2} a_i^{\dagger 2} a_i^2 + \Delta_i(t) a_i^{\dagger} a_i - \frac{p(t)}{2} (a_i^2 + a_i^{\dagger 2}) \right] + \hbar \xi(t) \left[- \sum_{i=1}^N \sum_{j=1}^N J_{i,j} a_i^{\dagger} a_j - A(t) \sum_{i=1}^N h_i (a_i + a_i^{\dagger}) \right], \quad (2)$$

where \hbar is the reduced Planck constant, a_i and a_i^{\dagger} are the annihilation and creation operators, respectively, for the i th KPO, K is the Kerr coefficient, $\Delta_i(t)$ is the detuning frequency for the i th KPO, $p(t)$ is the parametric pump amplitude, and $\xi(t)$ and $A(t)$ are control parameters [44]. In this work, we assume that all the parameters are positive (if not mentioned) [45]. Note that the above Hamiltonian is an *effective* one in a frame rotating at half the pump frequency and in the rotating-wave approximation [18, 20].

We increase $p(t)$ from zero to a sufficiently large value p_f (larger than K), decrease $\Delta_i(t)$ from $\Delta_i^{(0)}$ to zero, increase $\xi(t)$ from zero to a small value ξ_f (smaller than K), and set $A(t)$ as $A(t) = \sqrt{p(t)/K}$. Then, the initial and final Hamiltonians, H_0 and H_f , become

$$H_0 = \hbar \sum_{i=1}^N \left(\frac{K}{2} a_i^{\dagger 2} a_i^2 + \Delta_i^{(0)} a_i^{\dagger} a_i \right), \quad (3)$$

$$H_f = \hbar \frac{K}{2} \sum_{i=1}^N (a_i^{\dagger 2} - \alpha_f^2) (a_i^2 - \alpha_f^2) + \hbar \xi_f \left[- \sum_{i=1}^N \sum_{j=1}^N J_{i,j} a_i^{\dagger} a_j - \alpha_f \sum_{i=1}^N h_i (a_i + a_i^{\dagger}) \right], \quad (4)$$

where $\alpha_f = \sqrt{p_f/K}$ and a constant term, $-\hbar K \alpha_f^4/2$, has been dropped in Eq. (4).

From Eq. (3), we find that the initial ground state is exactly the vacuum state. On the other hand, the first term of H_f , which is positive semidefinite, has the degenerate ground states expressed as tensor products of coherent states with amplitudes $\pm \alpha_f$, $|\pm \alpha_f\rangle \cdots |\pm \alpha_f\rangle$ [46]. Thus,

assuming a sufficiently small ξ_f compared to K , the final ground state is approximately given by $|s_1 \alpha_f\rangle \cdots |s_N \alpha_f\rangle$, where $\{s_i = \pm 1\}$ minimizes the following energy:

$$E_f = 2\hbar \xi_f \alpha_f^2 \left(-\frac{1}{2} \sum_{i=1}^N \sum_{j=1}^N J_{i,j} s_i s_j - \sum_{i=1}^N h_i s_i \right). \quad (5)$$

Importantly, this is proportional to the Ising energy in Eq. (1): $E_f \propto E_{\text{Ising}}$. Consequently, we can obtain the solution of the Ising problem from the final state of the adiabatic evolution started with the vacuum state, assuming that $p(t)$ varies sufficiently slowly and the quantum adiabatic theorem holds.

To evaluate the ground-state AQC with KPOs, we solved 1000 random instances of the four-spin Ising problem, where we numerically solved the Schrödinger equation with the Hamiltonian in Eq. (2) (see Appendix A for the details of the simulation). The results are shown by the histograms in Figs. 1(a) and 1(b), where the failure probability is the probability that we fail to obtain the ground state of the Ising problem and the residual energy is the difference between the ground-state energy of the Ising problem and the expectation value of the Ising energy obtained by the AQC [47]. It is found that most instances are well solved by the ground-state AQC.

To magnify bad results, we plot the results in a two-dimensional plane, as shown in Fig. 1(c). It turns out that the ground-state AQC results in high failure probabilities or high residual energies in some instances. To examine the reason, we check the energy levels in a bad instance indicated by the vertical arrow in Fig. 1(c). (The details of this instance are provided in Appendix B and the numerical calculation of the energies is explained in Appendix C.) As shown in Fig. 1(d), the energy gap between the ground and first excited states almost closes at the point indicated by the vertical arrow. Thus, the reason for the bad result in this instance is attributed to this energy-gap closing. That is, the system is in the ground state before the energy-gap closing point. At this point, however, a nonadiabatic transition to the first excited state occurs. Consequently, we cannot obtain the ground state at the end. This time evolution is depicted by the dotted arrows in Fig. 1(d).

III. EXCITED-STATE AQC WITH KPOS

Here we present our proposed approach. To set the vacuum state to the first excited state of the initial Hamiltonian, we set one of the initial detunings, e.g. $\Delta_1^{(0)}$, to a negative value. Then, the single-photon and two-photon energies for the corresponding KPO at the initial time are expressed, respectively, as $\hbar \Delta_1^{(0)}$ and $\hbar(K + 2\Delta_1^{(0)})$. Thus, the vacuum state is the first excited state when $-K/2 < \Delta_1^{(0)} < 0$.

In the hard instance discussed in the last section, its energy levels change from the ones in Fig. 1(d) to the

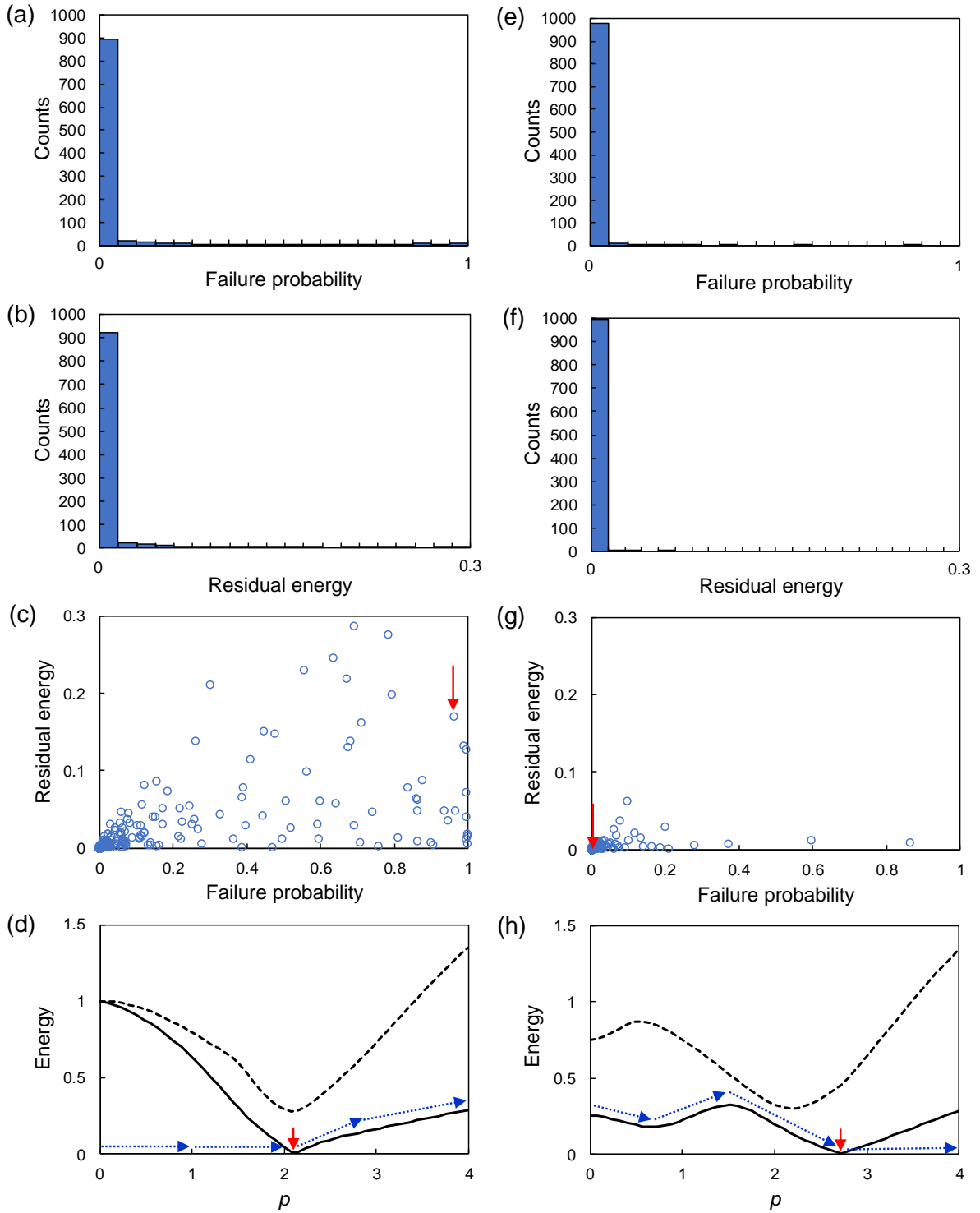


FIG. 1. Simulation results for 1000 random instances of the four-spin Ising problem. (See Appendix A for the details of the simulations.) $\{J_{i,j}\}$ and $\{h_i\}$ are set randomly from the interval $(-1, 1)$ and normalized by the maximum magnitude of them. (a)–(c) Results for the ground-state AQC with KPOs. (d) Energy levels from the ground-state energy as functions of pump amplitude p in the instance indicated by the vertical arrow in (c). Solid line: first excited state. Dashed line: second excited state. (See Appendix B for the details of the instance. Also see Appendix C for numerical calculation of the energies.) Here we use the units that $\hbar = 1$ and $K = 1$ (K and $\hbar K$ are the units of frequency and energy, respectively). Vertical arrow in (d) indicates energy-gap closing. Dotted arrows in (d) depict time evolution of the state during the AQC. (e)–(h) Corresponding results for the proposed approach using the excited-state AQC with KPOs.

ones in Fig. 1(h), where one of the initial detunings is set to $-K/4$ (the others are K). From Fig. 1(h), we expect to obtain the ground state via the nonadiabatic transition from the first excited state to the ground state at the energy-gap closing point, as depicted by the dotted arrows in Fig. 1(h). In fact, our simulation shows that the failure probability and the residual energy are improved from 0.963 and 0.171 to 7.10×10^{-4} and 6.87×10^{-4} , respectively, by the excited-state AQC, indicated by the vertical arrows in Figs. 1(d) and 1(h).

Note that the excited-state AQC does not always succeed. Our proposal is to try the ground-state AQC and the excited-state AQC with a negative $\Delta_i^{(0)}$ ($i = 1, \dots, N$) and to select the best result among the $(N + 1)$ cases. By this approach, the results for the 1000 random instances are dramatically improved from Figs. 1(a)–1(c) to Figs. 1(e)–1(g). This demonstrates the usefulness of the proposed approach.

IV. EFFECTS OF DISSIPATION

The merit of the present approach is the robustness of the initial state against errors due to dissipation. To demonstrate it, we solved the same instance as above by the ground-state and excited-state AQCs in the presence of dissipation (see Appendix A for the details of the simulation). For comparison, we also solved it by the excited-state AQC started with a really excited state, where one of the initial detunings is set to a positive value smaller than the others and the corresponding KPO is initially set in the single-photon state, resulting in the situation where the initial state is the first excited state. The energy levels in the case where one of the initial detunings is set to $K/4$ (the others are K) are shown in Fig. 2(a), from which we expect to successfully obtain the ground state via the nonadiabatic transition from the first excited state to the ground state at the energy-gap closing point, as depicted by the dotted arrows in Fig. 2(a).

The results for the three cases are shown in Fig. 2(b). (The success probability is one minus the failure probability.) As expected, the excited-state AQC started with a really excited state achieved a high success probability (0.9999) in the absence of dissipation ($\kappa = 0$). However, this performance is rapidly degraded as the decay rate κ increases. When κ is as large as $0.01K$, the excited-state AQC started with a really excited state becomes worse than the ground-state AQC. (The enhancement of the performance of the ground-state AQC by dissipation is explained by quantum heating [31].) On the other hand, the performance of the excited-state AQC started with vacuum states is more robust, as shown in Fig. 2(b). This result demonstrates the robustness of the present approach against errors due to dissipation.

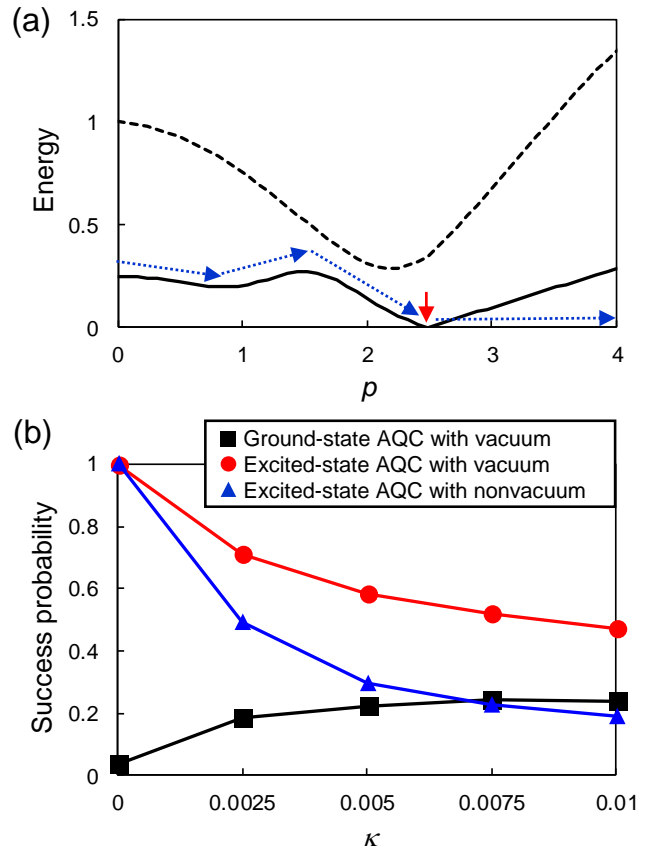


FIG. 2. Simulation results for a hard instance in the presence of dissipation. The instance is indicated by the vertical arrow in Fig. 1(c). (See Appendix B for the details of the instance.) (a) Energy levels from the ground-state energy as functions of pump amplitude p in the excited-state AQC started with a really excited (nonvacuum) state (see the main text). Solid line: first excited state. Dashed line: second excited state. (See Appendix C for numerical calculation of the energies.) Here, we use the units that $\hbar = 1$ and $K = 1$ (K and $\hbar K$ are the units of frequency and energy, respectively). Vertical arrow in (a) indicates energy-gap closing. Dotted arrows in (a) depict time evolution of the state during the AQC. (b) Success probability as a function of decay rate, κ , for photons in each KPO. Squares: ground-state AQC. Circles: excited-state AQC started with the vacuum state. Triangles: excited-state AQC started with a really excited state. See Appendix A for the details of the simulations.

V. CONCLUSIONS

We have proposed a new approach to excited-state AQC, which is started with not a really excited state, but the most stable state, namely, the vacuum state. This is based on the use of the effective Hamiltonian for a driven quantum system, that is, a KPO network, which allows one to set the vacuum state to an excited state for the Hamiltonian used for AQC. A hard instance, where the standard ground-state AQC ends up with failure because of energy-gap closing, can be solved by the excited-state

AQC exploiting a nonadiabatic transition from the first excited state to the ground state at an energy-gap closing point. Since the excited-state AQC is started with vacuum states, this AQC is robust against errors due to dissipation, which has been confirmed by numerical simulations. Thus, the present approach enhances the power of AQC and, in particular, offers a new way for tackling the energy-gap closing problem by harnessing a property of driven quantum systems.

ACKNOWLEDGMENTS

This work was supported by JST ERATO (Grant No. JPMJER1601).

Appendix A: Numerical simulations

To solve the four-spin Ising problem by AQCs with KPOs and to obtain the results in Figs. 1 and 2, we numerically solved the Schrödinger equation or the master equation with the Hamiltonian in Eq. (2):

$$\frac{d}{dt}|\psi\rangle = -\frac{i}{\hbar}H(t)|\psi\rangle, \quad (\text{A1})$$

$$\frac{d}{dt}\rho = -\frac{i}{\hbar}[H(t), \rho] + \kappa(2a\rho a^\dagger - a^\dagger a\rho - \rho a^\dagger a), \quad (\text{A2})$$

where $|\psi\rangle$ and ρ are the state vector and the density operator, respectively, describing the KPO network, $[O_1, O_2] = O_1O_2 - O_2O_1$ is the commutation relation between O_1 and O_2 , and κ is the decay rate for photons in each KPO. To solve the master equation numerically, we used the quantum-jump approach [48–50], where instead of the master equation (A2), we solve the Schrödinger equation with the non-Hermitian Hamiltonian:

$$\frac{d}{dt}|\psi\rangle = -\frac{i}{\hbar}H'(t)|\psi\rangle, \quad H'(t) = H(t) - i\hbar\kappa a^\dagger a. \quad (\text{A3})$$

The results in Fig. 2(b) were obtained by taking the averages over 1000 trials of the Monte-Carlo simulation in the quantum-jump approach.

In the numerical simulations, we truncated the Hilbert space for each KPO at a maximum photon number of 14, and represented the state vector $|\psi\rangle$ in the photon-number basis. The resultant differential equations were solved by the fourth-order Runge-Kutta method with a time step of $1/(500K)$.

In all the simulations, the parameters were set as follows (if not mentioned):

$$p(t) = p_f \sin \frac{\pi t}{2T}, \quad p_f = 4K, \quad (\text{A4})$$

$$\Delta_i(t) = \Delta_i^{(0)} \cos \frac{\pi t}{2T}, \quad \Delta_i^{(0)} = K, \quad (\text{A5})$$

$$\xi(t) = \xi_f \sin \frac{\pi t}{2T}, \quad \xi_f = \frac{K}{4}, \quad (\text{A6})$$

where $T = 400/K$ is the computation time of the AQCs.

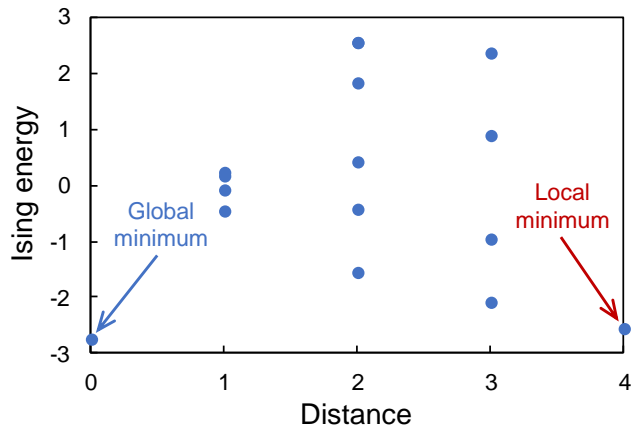


FIG. 3. Energy landscape of the hard instance [indicated by the vertical arrow in Fig. 1(c)]. “Distance” is the Hamming distance between the optimal solution (the global minimum) and each configuration [51].

Appendix B: Details of the hard instance

The coupling coefficients and the local fields of the instance used for Figs. 1(d), 1(h), and 2 [indicated by the vertical arrow in Fig. 1(c)] are defined as follows:

$$\begin{aligned} J_{1,2} &= J_{2,1} = 0.266654, \\ J_{1,3} &= J_{3,1} = 0.886155, \\ J_{1,4} &= J_{4,1} = 0.019833, \\ J_{2,3} &= J_{3,2} = 0.071362, \\ J_{2,4} &= J_{4,2} = -0.446931, \\ J_{3,4} &= J_{4,3} = -1, \\ h_1 &= -0.340697, \\ h_2 &= -0.546404, \\ h_3 &= 0.501731, \\ h_4 &= -0.296651. \end{aligned}$$

The energy landscape of this instance is depicted in Fig. 3. It is found that there is a nonglobal local minimum far from the global minimum. This may be the reason why this instance is hard.

Appendix C: Numerical calculation of energies

The energies in Figs. 1(d), 1(h), and 2(a) are obtained by diagonalizing the Hamiltonian matrix. However, the size of this matrix ($15^4 \times 15^4$ in the present case) is too large to directly diagonalize. Instead of the direct diagonalization, we calculated the energies as follows.

We first numerically obtain the eigenvectors for each KPO by diagonalizing each term in the first term of $H(t)$ in Eq. (2). Taking N_e eigenvectors from low energies as a basis, we obtain a $N_e^4 \times N_e^4$ matrix representation of $H(t)$. Finally, we diagonalize this matrix and obtain the

energies. Note that we can obtain the exact diagonalization if we take all the basis vectors ($N_e = 15$). To reduce the computational costs, we set $N_e = 6$ in the present calculations, because the energies obtained sufficiently

converge. This approach based on the low-energy approximation is valid when ξ is small compared to K , as in the present case.

-
- [1] E. Farhi, J. Goldstone, S. Gutmann, and M. Sipser, *Quantum Computation by Adiabatic Evolution*, arXiv:quant-ph/0001106.
- [2] E. Farhi, J. Goldstone, S. Gutmann, J. Lapan, A. Lundgren, and D. Preda, *A Quantum Adiabatic Evolution Algorithm Applied to Random Instances of an NP-Complete Problem*, *Science* **292**, 472 (2001).
- [3] T. Albash and D. A. Lidar, *Adiabatic Quantum Computation*, *Rev. Mod. Phys.* **90**, 015002 (2018).
- [4] T. Kadowaki and H. Nishimori, *Quantum Annealing in the Transverse Ising Model*, *Phys. Rev. E* **58**, 5355 (1998).
- [5] G. E. Santoro, R. Martoňák, E. Tosatti, and R. Car, *Theory of Quantum Annealing of an Ising Spin Glass*, *Science* **295**, 2427 (2002).
- [6] A. Das and B. K. Chakrabarti, *Colloquium: Quantum Annealing and Analog Quantum Computation*, *Rev. Mod. Phys.* **80**, 1061 (2008).
- [7] *Metaheuristics*, edited by P. Siarry (Springer International Publishing, 2016).
- [8] F. Barahona, *On the Computational Complexity of Ising Spin Glass Models*, *J. Phys. A* **15**, 3241 (1982).
- [9] A. Lucas, *Ising Formulations of Many NP Problems*, *Front. Phys.* **2**, 5 (2014).
- [10] F. Barahona, M. Grötschel, M. Jünger, and G. Reinelt, *An application of combinatorial optimization to statistical physics and circuit layout design*, *Operations Research* **36**, 493–513 (1988).
- [11] H. Sakaguchi, K. Ogata, T. Isomura, S. Utsunomiya, Y. Yamamoto, and K. Aihara, *Boltzmann sampling by degenerate optical parametric oscillator network for structure-based virtual screening*, *Entropy* **18**, 365 (2016).
- [12] G. Rosenberg, P. Haghnegahdar, P. Goddard, P. Carr, K. Wu, and M. L. de Prado, *Solving the optimal trading trajectory problem using a quantum annealer*, *IEEE J. Selected Topics in Signal Processing* **10**, 1053-1060 (2016).
- [13] A. Messiah, *Quantum Mechanics, Vol. II* (North-Holland Publishing Company, Amsterdam, 1962).
- [14] R. D. Somma, D. Nagaj, and M. Kieferová, *Quantum Speedup by Quantum Annealing*, *Phys. Rev. Lett.* **109**, 050501 (2012).
- [15] S. Bravyi, D. P. Divincenzo, R. Oliveira, and B. M. Terhal, *The Complexity of Stoquastic Local Hamiltonian Problems*, *Quantum Inf. Comput.* **8**, 0361 (2008); arXiv:quant-ph/0606140.
- [16] S. P. Jordan, D. Gosset, and P. J. Love, *Quantum-Merlin-Arthur-Complete Problems for Stoquastic Hamiltonians and Markov Matrices*, *Phys. Rev. A* **81**, 032331 (2010).
- [17] E. Crosson, E. Farhi, C. Y.-Y. Lin, H.-H. Lin, and P. Shor, *Different Strategies for Optimization Using the Quantum Adiabatic Algorithm*, arXiv:1401.7320.
- [18] H. Goto, *Bifurcation-Based Adiabatic Quantum Computation with a Nonlinear Oscillator Network*, *Sci. Rep.* **6**, 21686 (2016).
- [19] H. Goto, *Universal Quantum Computation with a Nonlinear Oscillator Network*, *Phys. Rev. A* **93**, 050301(R) (2016).
- [20] H. Goto, *Quantum Computation Based on Quantum Adiabatic Bifurcations of Kerr-Nonlinear Parametric Oscillators*, *J. Phys. Soc. Jpn.* **88**, 061015 (2019).
- [21] Z. Wang, A. Marandi, K. Wen, R. L. Byer, and Y. Yamamoto, *Coherent Ising machine based on degenerate optical parametric oscillators*, *Phys. Rev. A* **88**, 063853 (2013).
- [22] A. Marandi, Z. Wang, K. Takata, R. L. Byer, and Y. Yamamoto, *Network of time-multiplexed optical parametric oscillators as a coherent Ising machine*, *Nat. Photon.* **8**, 937-942 (2014).
- [23] Y. Yamamoto, K. Aihara, T. Leleu, K. Kawarabayashi, S. Kako, M. Fejer, K. Inoue, and H. Takesue, *Coherent Ising machines optical neural networks operating at the quantum limit*, *npj Quantum Inf.* **3**, 49 (2017).
- [24] N. Bartolo, F. Minganti, W. Casteels, and C. Ciuti, *Exact Steady State of a Kerr Resonator with One- and Two-Photon Driving and Dissipation: Controllable Wigner-Function Multimodality and Dissipative Phase Transitions*, *Phys. Rev. A* **94**, 033841 (2016).
- [25] Y. Zhang and M. I. Dykman, *Preparing Quasienergy States on Demand: A Parametric Oscillator*, *Phys. Rev. A* **95**, 053841 (2017).
- [26] S. Puri, S. Boutin, and A. Blais, *Engineering the Quantum States of Light in a Kerr-Nonlinear Resonator by Two-Photon Driving*, *npj Quant. Inf.* **3**, 18 (2017).
- [27] S. E. Nigg, N. Lörch, and R. P. Tiwari, *Robust Quantum Optimizer with Full Connectivity*, *Sci. Adv.* **3**, e1602273 (2017).
- [28] S. Puri, C. K. Andersen, A. L. Grimsmo, and A. Blais, *Quantum Annealing with All-to-All Connected Nonlinear Oscillators*, *Nat. Commun.* **8**, 15785 (2017).
- [29] V. Savona, *Spontaneous Symmetry Breaking in a Quadratically Driven Nonlinear Photonic Lattice*, *Phys. Rev. A* **96**, 033826 (2017).
- [30] P. Zhao, Z. Jin, P. Xu, X. Tan, H. Yu, and Y. Yu, *Two-Photon Driven Kerr Resonator for Quantum Annealing with Three-Dimensional Circuit QED*, *Phys. Rev. Applied* **10**, 024019 (2018).
- [31] H. Goto, Z. Lin, and Y. Nakamura, *Boltzmann Sampling from the Ising Model Using Quantum Heating of Coupled Nonlinear Oscillators*, *Sci. Rep.* **8**, 7154 (2018).
- [32] M. I. Dykman, C. Bruder, N. Lörch, and Y. Zhang, *Interaction-Induced Time-Symmetry Breaking in Driven Quantum Oscillators*, *Phys. Rev. B* **98**, 195444 (2018).
- [33] H. Goto, Z. Lin, T. Yamamoto, and Y. Nakamura, *On-Demand Generation of Traveling Cat States Using a Parametric Oscillator*, *Phys. Rev. A* **99**, 023838 (2019).
- [34] R. Rota, F. Minganti, C. Ciuti, and V. Savona, *Quantum Critical Regime in a Quadratically Driven Nonlinear Photonic Lattice*, *Phys. Rev. Lett.* **122**, 110405 (2019).

- [35] Z. Wang, M. Pechal, E. A. Wollack, P. Arrangoiz-Arriola, M. Gao, N. R. Lee, and A. H. Safavi-Naeini, *Quantum Dynamics of a Few-Photon Parametric Oscillator*, Phys. Rev. X **9**, 021049 (2019).
- [36] S. Puri, A. Grimm, P. Campagne-Ibarcq, A. Eickbusch, K. Noh, G. Roberts, L. Jiang, M. Mirrahimi, M. H. Devoret, and S. M. Girvin, *Stabilized Cat in a Driven Nonlinear Cavity: A Fault-Tolerant Error Syndrome Detector*, Phys. Rev. X **9**, 041009 (2019).
- [37] A. Grimm, N. E. Frattini, S. Puri, S. O. Mundhada, S. Touzard, M. Mirrahimi, S. M. Girvin, S. Shankar, and M. H. Devoret, *The Kerr-Cat Qubit: Stabilization, Readout, and Gates*, arXiv:1907.12131.
- [38] S. Puri, L. St-Jean, J. A. Gross, A. Grimm, N. E. Frattini, P. S. Iyer, A. Krishna, S. Touzard, L. Jiang, A. Blais, S. T. Flammia, and S. M. Girvin, *Bias-Preserving Gates with Stabilized Cat Qubits*, arXiv:1905.00450.
- [39] R. Y. Teh, F.-X. Sun, R. E. S. Polkinghorne, Q. Y. He, Q. Gong, P. D. Drummond, and M. D. Reid, *Dynamics of Transient Cat States in Degenerate Parametric Oscillation with and without Nonlinear Kerr Interactions*, Phys. Rev. A **101**, 043807 (2020).
- [40] W. Verstraelen and M. Wouters, *Classical Critical Dynamics in Quadratically Driven Kerr Resonators*, Phys. Rev. A **101**, 043826 (2020).
- [41] D. Roberts and A. A. Clerk, *Driven-Dissipative Quantum Kerr Resonators: New Exact Solutions, Photon Blockade and Quantum Bistability*, Phys. Rev. X **10**, 021022 (2020).
- [42] M. J. Kewming, S. Shrapnel, and G. J. Milburn, *Quantum correlations in the Kerr Ising model*, New J. Phys. **22**, 053042 (2020).
- [43] In this work, we assume time-dependent Δ_i and ξ , unlike the literature [18, 20, 31], for convenience of the extension to the excited-state AQC.
- [44] ξ has the dimension of frequency and A is dimensionless.
- [45] In superconducting-circuit implementations, K is usually negative. In this case, we set the other parameters except A to be negative. Then, we obtain the same results [20].
- [46] A coherent state $|\alpha\rangle$ is defined as an eigenstate of the annihilation operator a : $a|\alpha\rangle = \alpha|\alpha\rangle$.
- [47] The probabilities for the spin configurations are calculated by the method in Ref. [18].
- [48] M. O. Scully and M. S. Zubairy, *Quantum Optics* (Cambridge University Press, Cambridge, 1997).
- [49] H.-P. Breuer and F. Petruccione, *The Theory of Open Quantum Systems* (Oxford University Press, Oxford, 2002).
- [50] M. B. Plenio and P. L. Knight, *The Quantum-Jump Approach to Dissipative Dynamics in Quantum Optics*, Rev. Mod. Phys. **70**, 101 (1998).
- [51] The Hamming distance between two spin configurations, $\{s_i\}$ and $\{s'_i\}$, is defined by the number of spin pairs, (s_i, s'_i) , satisfying $s_i \neq s'_i$.